2015

Parametric investigation of the mechanics of soft-body contact with parallel-ridge textured surfaces to understand tactile friction

Thomas Joseph Wilde
Iowa State University

Parametric investigation of the mechanics of soft-body contact with parallel-ridge textured surfaces to understand tactile friction

by

Thomas Joseph Wilde

A thesis submitted to the graduate faculty

in partial fulfillment of the requirements for the degree of

MASTER OF SCIENCE

Major: Mechanical Engineering

Program of Study Committee:
Christian Schwartz, Major Professor
Adarsh Krishnamurthy
Thomas Rudolphi

Iowa State University

Ames, Iowa

2015

TABLE OF CONTENTS

LIST OF FIGURES

Page

ACKNOWLEDGEMENTS

I would like to give thanks to my committee chair, Dr. Schwartz, for the guidance, patience, and knowledge he has shown me. I would also like to thank Dr. Krishnamurthy, Dr. Wei, and Dr. Rudolphi for their willingness to participate on my committee and additionally thank Dr. Shrotriya and Dr. Wei for the guidance they have provided in coursework studies.

I would especially like to thank my parents, my grandfather, and the rest of my friends and family for the support that they have provided throughout my life.

ABSTRACT

Tactile friction which occurs between the surfaces of hand-operated products and the user as well as the user's perception of surface characteristics are both very important considerations for the function of engineering products. While the use of surface texture is known to greatly influence these properties, the effect of the governing textural parameters on the friction mechanisms between a textured material and a deformable material is poorly understood making it difficult to design textures for specific tactile properties. The ability to model the tactile outcomes for the interaction between a simple textured surface and deformable body would be very beneficial to understanding how friction coefficient and perception of textures are influenced.

Previous studies have measured friction between polymers and textures, obtained qualitative data of subject perceptions of surface topographies, and have used computational simulations to better understand the underlying friction and perception mechanisms. It has previously been hypothesized that the penetration of the deformable material into the valleys of a surface texture drives friction behavior. Two dimensional profiles of simple textures are often examined to more easily isolate the effects of textural parameters. In this investigation, an elastic mechanics based computational model was developed to predict the behavior between a cylindrical deformable material against a rigid body of rectangular grooves. A non-dimensionalized similitude approach was used to investigate the dependence of groove penetration and the number of ridges in contact on groove and ridge dimension, as well as applied pressure and the elastic modulus. The penetration computational results were verified by a macro-scale empirical investigation and groove contact computational results

were compared to predictions based on Hertzian contact between a cylinder and a rigid flat plane. It was found that groove and ridge dimensions have a very profound effect on the penetration behavior of the elastomeric body. Smaller grooves and wider ridges resulted in a negligible difference on ridges in contact from the Hertzian contact prediction. However, as groove size increased and ridge width decreased, an empirical computational model was developed which accurately predicted ridges in contact.

CHAPTER I

INTRODUCTION

The interaction between the surface of a hand-operated product and the user can be essential to the functionality of the product. The ability to design for such a response has gained a lot of recent interest with the development of new products with greater functionality. However, tactile perception and friction of various surface topographies is a complex phenomenon that is still poorly understood. Rudimentary knowledge of this interaction allows engineers to design surfaces that generally serve their purpose, from grips on tools, electronics, bottles, and toiletries, to the textures of rails, sidewalk ramps, stairs, and shower floors. Mobile phone buttons are now designed with different textures so that the user can tactually distinguish between their functions. Other designs such as car interiors serve to elicit a positive emotional response such as having a leather-like feel. The realization of the importance of surface qualities necessitates the ability to better quantify these interactions so that frictional characteristics can be more accurately obtained through engineering design. Current investigations involve tracking the frictional response to skin-like rubbers under loading conditions with various counter surfaces as well as qualitative analyses testing subjects' abilities to distinguish between different surfaces based on parameters such as average surface roughness or distance between surface asperities. More recently the use of finite element analysis (FEA) has been utilized to analyze stresses within the skin layers and determine how coefficient of friction (COF) or surface characteristics influence tactile perception based on the locations of high stress relative to tactile nerve receptors.

It is hypothesized in this thesis that penetration of a deformable body into the valleys of a surface texture is a major driving force for frictional properties. In addition, the possibility of adhesion between the deformable body and the bottom of grooves of the textured surface is of great interest. The first investigation utilizes a series of computational simulations of a cylindrical deformable body being loaded against a two dimensional rigid rectangular-ridged texture. Through the regression of the collected penetration data, a model was developed to predict penetration based on groove and ridge widths as well as applied pressure and elastic modulus. The model was then verified using an empirical macro scale investigation of elastomer cylinders loaded against a constructed groove.

The dependence of adhesive friction on real contact area is well documented. Additionally, friction has been seen to increase with surface roughness at higher roughness values due to an interlocking component. With the hypothesis of penetration being a driving force for frictional characteristics, the number of grooves in which penetration exists is of great interest for the development of an interlocking model. Predicting the number of ridges in contact with a deformable body is also useful for determining real contact area. However, it remains unknown if Hertzian contact between a cylinder and a flat rigid plan is an adequate approximation to determining the number of ridges which come into contact with a deformable cylinder. In the second investigation, computational simulations were conducted to model the contact between a parallel rectangular-grooved surface and a cylindrical deformable body. The Hertzian model for contact distance was modified to incorporate texture parameters and used to analytically predict the number of ridges in contact. In the computational simulations, the load at which each addition ridge came into contact was noted for several ridge and groove dimensions.

A regression model was developed from the collected load data and the validity of the Hertzian contact approximation in reference to a grooved surface was addressed.

CHAPTER II

PARAMETRIC INVESTIGATION OF SOFT-BODY PENETRATION INTO PARALLEL-RIDGE TEXTURED SURFACES

A paper to be submitted to the *International Journal of Solids and Structures*

T.J. Wilde, C.J. Schwartz

2.1 Introduction

Tactile friction and perception are of great interest to engineers and product designers because of the number of products which are handled every day that require suitable surface characteristics to serve their function or to please the user. Perception enables us to judge characteristics of materials that we interact with whether they are cosmetic or functional. On the cosmetic side, tactile perception has been shown to influence our perception and feeling towards products [1-3]. On the other hand, the frictional components of tactile perception can allow us to distinguish between materials [4] and indicate to us if we need to apply more or less force when handling an object whether to influence grip or reduce abrasion. Thus, engineered surfaces are often optimized for their frictional purposes. For example, low friction surfaces such as the mouse pad of a laptop allow for ease of movement while high friction surfaces such as tool handles, phone cases, railing, and gym weights are all designed to give the user grip.

It has been shown that tactile friction can be reasonably modeled as a summation of friction from adhesion and deformation [5], adhesion being the dominant mechanism [5, 6]. Experiments have shown that coefficient of friction decreases as surface roughness is increased from a nominally smooth surface [7, 8]. This has been attributed to a reduction in real contact area reducing the amount of adhesion between the two surfaces. However, once a certain

roughness is achieved the friction increases sharply. Tomlinson et al. [9] experimented with triangular ridged surfaces of varying sizes and showed that when the surface roughness was increased to a certain threshold, an increase in friction was seen. This was attributed to an increase of the deformation component of friction by viscoelastic hysteresis and interlocking. They also noted that when groove depth was shallow, adhesion still occurred because the penetration of the finger into the grooves had reached the bottom of the groove channels. Darden et al. [10] hypothesized about the same phenomenon when testing the effect of sliding direction on friction against parallel-ridge textures. They investigated the sliding of a spherical neoprene probe parallel to and perpendicular to the orientation of ridges on a simple parallel-ridge textured surface. When the textural ridges were below a certain height, the coefficient of friction did not exhibit a change with sliding orientation, whereas ridges above this height showed a marked sliding orientation effect. Taylor and Lederman showed that the penetration of the finger into the groove is also an important factor in perception of roughness and developed a model to predict perceived surface roughness of parallel ridged surfaces as a function of penetration, groove width, and finger force [11]. Correlations have been found between perceived roughness and friction [1, 4, 12]. Numerous studies have also shown an increase in perceived roughness as groove width increases [12-14] which plays a crucial role in the amount of penetration that occurs.

The mechanics at the finger-on-texture interface are very complex. However, finite element analysis (FEA) has been utilized to model the interaction between fingers and surfaces to account for the complexities of the interaction and to analyze the stresses produced within the finger. Xydas et. al [15] utilized FEA to determine the effect of adhesive friction on contact area of a finger on a flat surface using experimental friction measurements. Maeno et. al [16] utilized

FEA to model the internal stresses within the finger during movement along a flat surface taking into account the epidermal ridges, papillae, and bone and found that tactile receptors are appropriately located in areas of maximum von Mises stress produced by the shearing of the epidermal ridges. Shao et al. [17] conducted a similar FEA study analyzing the effect of epidermal ridges on the oscillation of friction force and location of maximum von Mises stress when the finger interacts with a textured surface.

Because of the observed impact on friction coefficient of fingertip penetration into textural features, this investigation sought to better understand the mechanics of the penetration of the finger into textural grooves because of its importance in designing textures with desired levels of friction or perceived roughness. Accurately predicting the amount of penetration into textural grooves would help to predict the likelihood of micro-adhesion at the bottom of the groove channels, provide insight into the perception of surface roughness, and possibly provide insight into predicting the amount of friction due to deformation. There currently lacks an analytical solution, such as those presented by Hertz for the contact distance of a cylinder against a rigid plane, for the penetration of a cylinder as it's compressed against a rigid grooved surface.

The objective of this study was to develop a model to predict the amount of penetration of a soft cylindrical body into a rigid parallel rectangular grooved surface to simulate finger-on-texture contact. The parameters considered in this interaction included the widths of the surface grooves and ridges as well as the radius of the cylinder, elastic modulus, and applied pressure. Parameters of similitude were non-dimensionalized with one another as input variables to make the model applicable to both the micro and macro scale. An analytical mechanical approach was taken as a basis of the relationship between applied load and penetration. A computational model was developed by the regression of the penetration results of numerous FE simulations which

varied the groove width in a particular range of interest applicable to the surface textures used in experiments of Darden et al. [10]. The effect of multiple grooves on penetration was also analyzed in order to better model realistic textures.

2.2 Methods

The methodology of this investigation was to develop a model to predict penetration of an elastomeric cylindrical body into rectangular rigid grooves based on textural geometry parameters and elastomer stiffness. To attain this goal, an FE model of both the cylinder and texture were developed and studied. FE results were compared to data collected from an experimental apparatus in order to validate the FE model, and finally the effects of additional grooves were studied using the model. The dimensionless parameters of the model were determined by dimensional analysis (Buckingham Pi theorem) and the structure of the model was determined both by an analytical technique and using a least squares regression to several data resulting from numerous FEA simulations.

2.2.1 Texture parameters and similitude approach

The modelled textures were two-dimensional parallel ridges with rectangular cross section. The space between the ridges (referred to as 'grooves') is referred to as 'b', while ridge width is referred to as 'a'. The cylinder, which was loaded into the texture, is defined by its radius, R, elastic modulus, E, and Poisson ratio, ν. A load was applied to a rigid horizontal plate which rested above the cylinder. The applied load per unit length, divided by the cylinders diameter is denoted by 'p'. The output parameter of interest is the total penetration of the

cylinder into the central groove, δ_{tot}. The total penetration is a combination of the initial penetration, δ_i, as the cylinder rests atop the central groove without any external loading, and the forced penetration, δ_f, which is the penetration caused from the applied loading. The initial penetration (based solely on cylinder radius and groove width) was calculated using trigonometry of a circle of radius, R, resting atop two ridges with a fillet radius, r, spaced a distance, b. This initial penetration, δ_i, can be calculated by

$$\delta_i = R + r - \sqrt{\left(R+r\right)^2 - \left(\frac{b}{2}+r\right)^2} \tag{1}$$

While the fillet radius affects δ_i, for the purpose of this experiment, it is assumed to be small enough to have a negligible effect on δ_f. Fig. 1 shows both the uncompressed and compressed state of a cylinder interacting with a grooved surface. Dimensionless parameters of similitude were selected as input parameters for the model through the use of Buckingham Pi theorem. From these parameters, there were two dimensions including length and force. This left the unique variables in each Π term to be δ_f, p, and b, respectively. The use of dimensional analysis

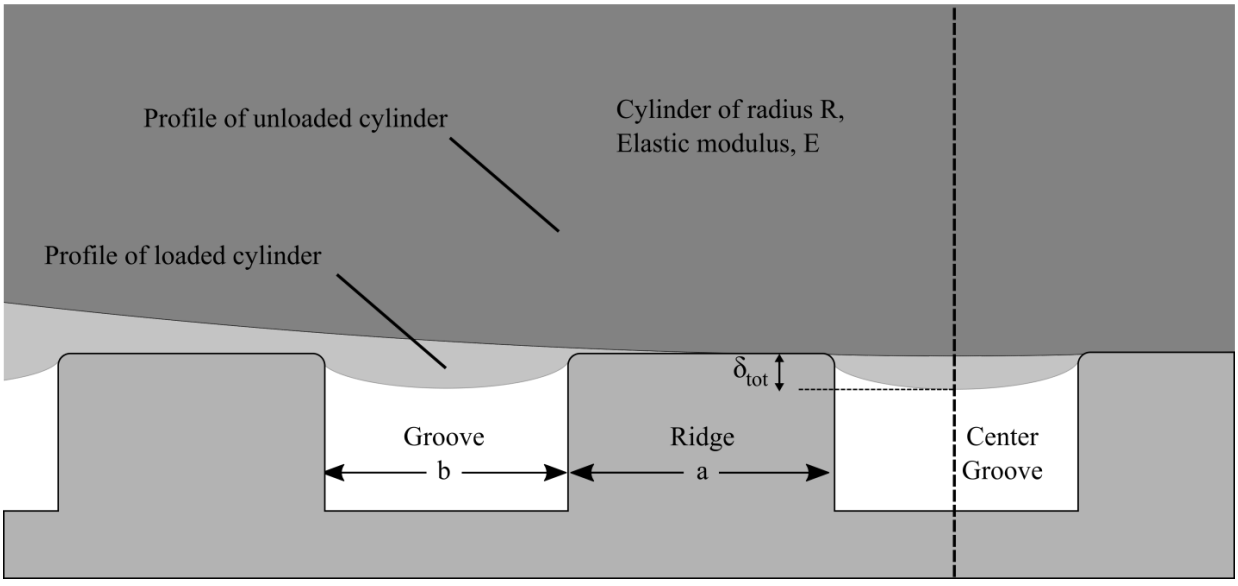

Fig. 1. Depiction of the parameters which govern the penetration of a soft cylinder into a rigid grooved surface.

yielded the output dimensionless parameter involving penetration, δ_f/R, and the input parameters p/E and b/R which depend on load, geometry and material properties. The contribution from each input parameter was determined by the analytical and FEA methods in the following sections.

2.2.2 Mechanics basis for finite element approach

In an attempt to determine an analogous phenomenon that possessed a closed-form analytical solution to serve as the basis of a regression model, the penetration of the cylinder into the grooved rigid body was modeled by the compression of parallel infinitesimal springs that made up the body of the cylinder between a rigid plate and a single rigid groove. Although this one-dimensional simplification ignored the transverse behavior due to shear and Poisson effects, it provided a useful overarching conceptual framework. Fig. 2 illustrates this parallel-spring model. The total compression of the cylinder, c, is equal to the distance the center spring penetrates into the groove. The compression of an individual spring, c_s, is equal to the difference in length between the length of the spring, L_s, and the center spring, L_{cs}, subtracted from $2c$ or

$$c_s = 2c - \left(L_{cs} - L_s\right) \tag{2}$$

L_{cs} is equal to $2R$, and L_s was determined by geometry and the spring's horizontal distance from the center, x_s. Equation 2 then becomes

$$c_s = 2c - \left(2R - 2\sqrt{R^2 - x_s^2}\right) \tag{3}$$

Assuming the same spring constant for each spring, the resulting force for a given compression is a function of the summation of the compressions of all springs in contact with the rigid plates and normalized by the number of finite springs. This can be seen by

$$force \sim \sum_{s=s_b}^{s=s_d} \frac{2c - 2R + 2\sqrt{R^2 - x_s^2}}{\#\,Springs} \tag{4}$$

where s_b is the first spring in contact with the base plate located at half the groove width from the center of the circle and s_d is the last spring in contact with both the pressing plate and base. Each spring's position, x_s, was determined by the even distribution of springs along the diameter of the circle. The spring was considered to be in contact if the absolute value of its position was greater than half of the groove width and within the half-contact distance, d_h, which is determined by geometry and c to be

$$d_h = \sqrt{2Rc - c^2} \tag{5}$$

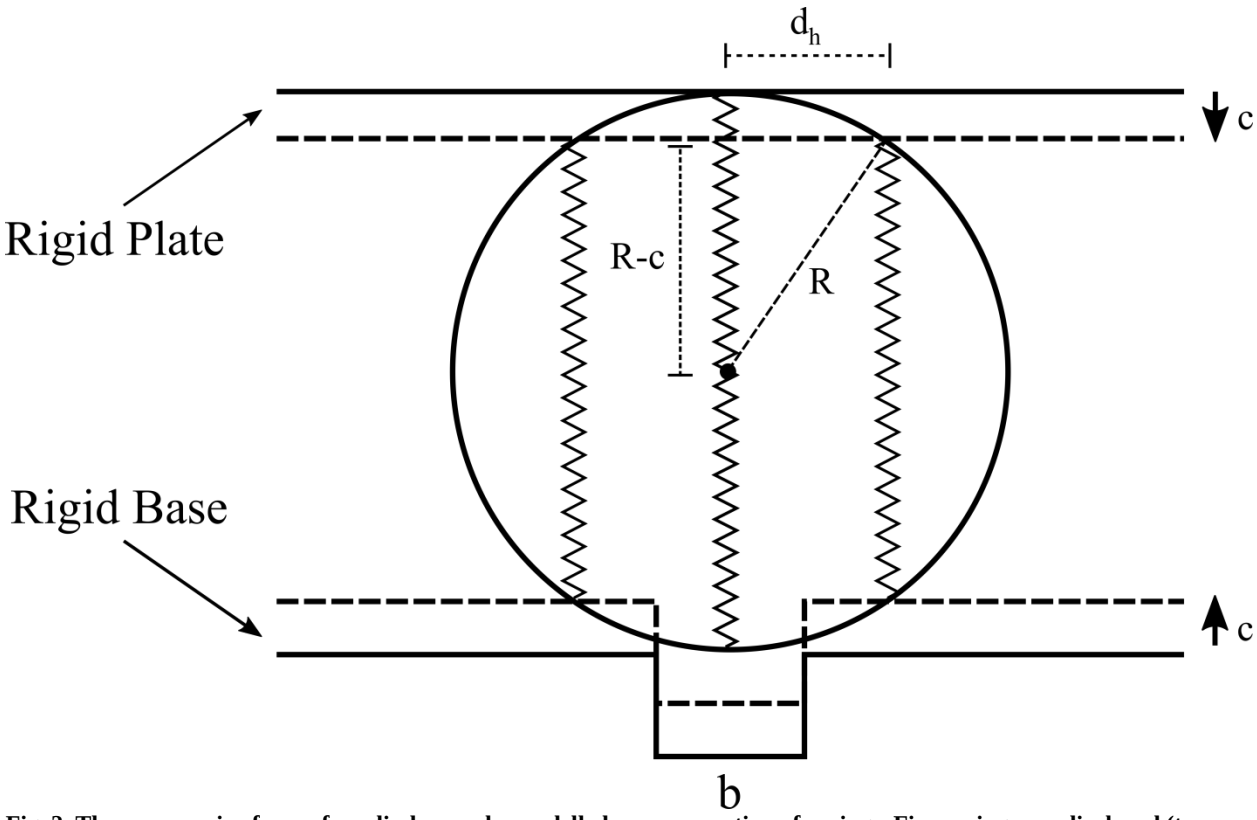

Fig. 2. The compressive force of a cylinder can be modelled as a summation of springs. Five springs are displayed (two are infinitely small at the sides of the cylinder). Contact distance is calculated using Pythagorean theorem.

This approach is shown in the figure, but with only three springs displayed for simplicity. Solutions to (4) were determined by using a computational algorithm, and a least squares regression was used to determine the direct relationship between the compression of a cylinder and the resulting force.

2.2.3 Finite element model

A two-dimensional FEA model (Abaqus/CAE v6.12) was constructed to investigate the relationship between the applied load on a cylindrical body resting on a single grooved rigid body and the resultant forced penetration, $\delta_{f,}$ into the groove as seen by Fig. 3. An 8-node biquadratic plain strain quadrilateral element was used with full integration. Plain strain elements were chosen because deformation outside of the plane was assumed to be negligible for both tactile studies and the experimental apparatus consisting of a long polyurethane cylinder.

The cylinder was modeled to be linearly elastic and inertial effects were neglected. The Poisson ratio, ν, was set to 0.49 to model nearly incompressible behavior. The ratio of groove width to cylinder radius (*b/R)* was varied from 0.01 to 0.1 in increments of 0.01. The ratio of load per unit area to elastic modulus (*p/E)* was varied from 0 to 0.03 in a total of 1000 increments or until excessive deformation occurred at which point model solution iteration could not proceed. The selected *b/R* range was of particular interest because it incorporated the range of groove sizes used in tactile friction experiments used by Darden et al. Moreover, this particular range targeted the hypothesized threshold of the human ability to discriminate gaps as indicated by Johnson et al. [18] assuming the finger is modelled as a cylinder with a diameter equal to the short axis of the finger as measured by Maeno et al. [16].

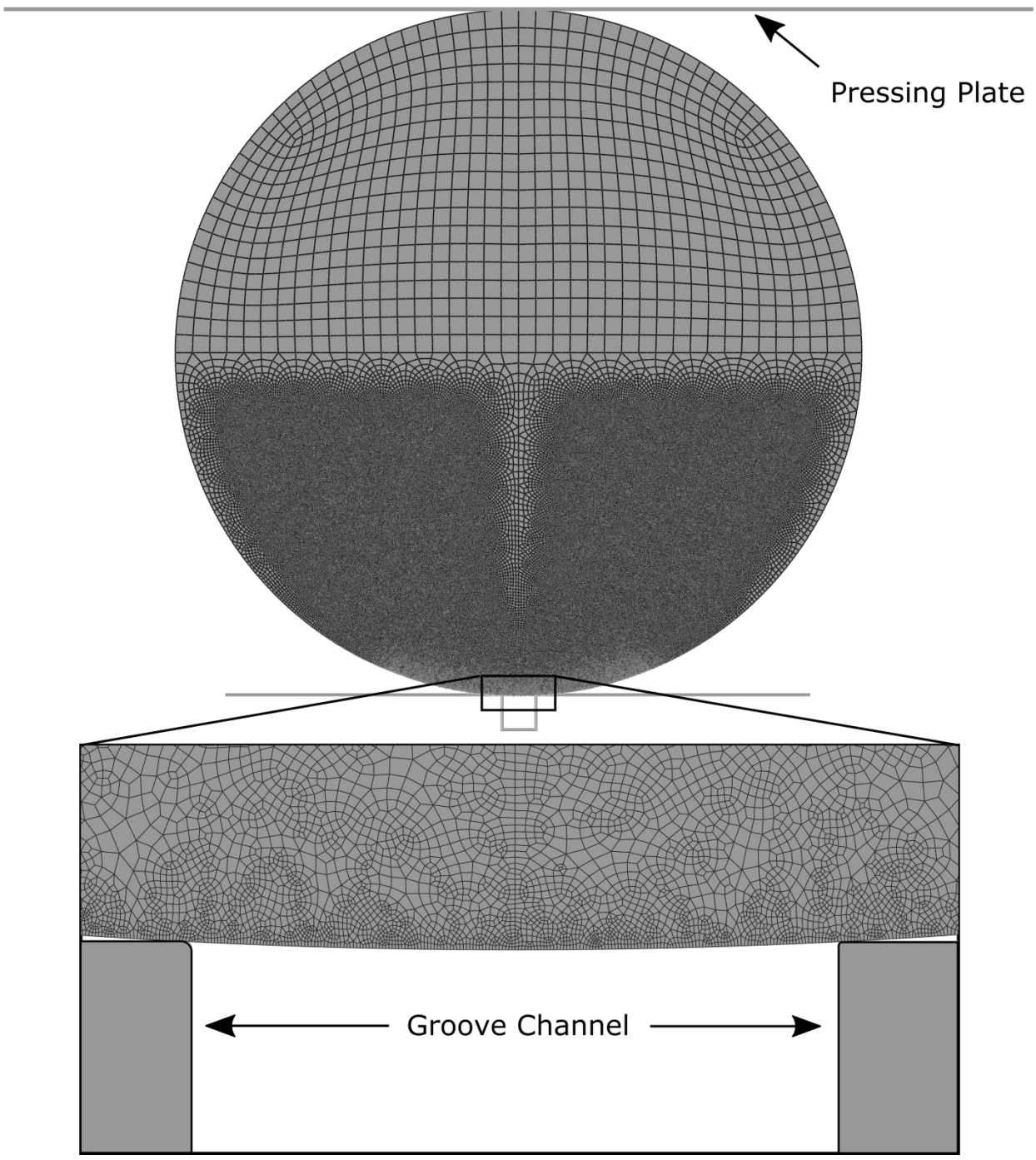

Fig. 3. Overview of assembly with detail of refined mesh near groove with *b*/*R* equal to 0.1.

A static implicit step was used in the FE approach with a history output tracking the location of the center node of the bottom surface of the cylinder. This history output enforced a penetration calculation at 1000 intervals of the total load. A constraint was placed on the vertical centerline of the circle to prevent movement in the x direction which both kept the object stable and allowed for accurate penetration calculations. The adhesive coefficient of friction between the interacting surfaces was set to 0 to focus solely on the effect of geometry and load. After the FE model was physically validated (see below), simulations were run with additional grooves to determine their effect on penetration. These simulations were run on all combinations of 3, 5, and 7 grooves with b/R values of 0.01, 0.02, 0.03 and a/R values of 0.012, 0.022, and 0.032.

2.2.4 Physical validation of numerical model

An experimental apparatus was built in order to collect penetration data to validate the FE model results. Because the FEA model used dimensionless parameters of similitude, the physical apparatus was able to be constructed on the macro scale, allowing the penetration to be easily measured. The apparatus consisted of a steel plate which was mounted on four rods with linear bearings which allowed for displacement in the vertical direction as shown by Fig. 4, and three different polyurethane cylinders with varying elastic moduli. The polyurethane cylinder rested atop two aluminum blocks which were displaced a desired distance and fixed in order to model two ridges separated by a groove. The area on the top of the pressing plate allowed for the use of calibration weights to be stacked for load application. Once loaded, a digital microscope (AM2111 Dino-Lite Basic) was used to acquire images of the front face of the polyurethane cylinder. These images were then analyzed using image analysis software (ImageJ 1.48) to determine total penetration into the groove.

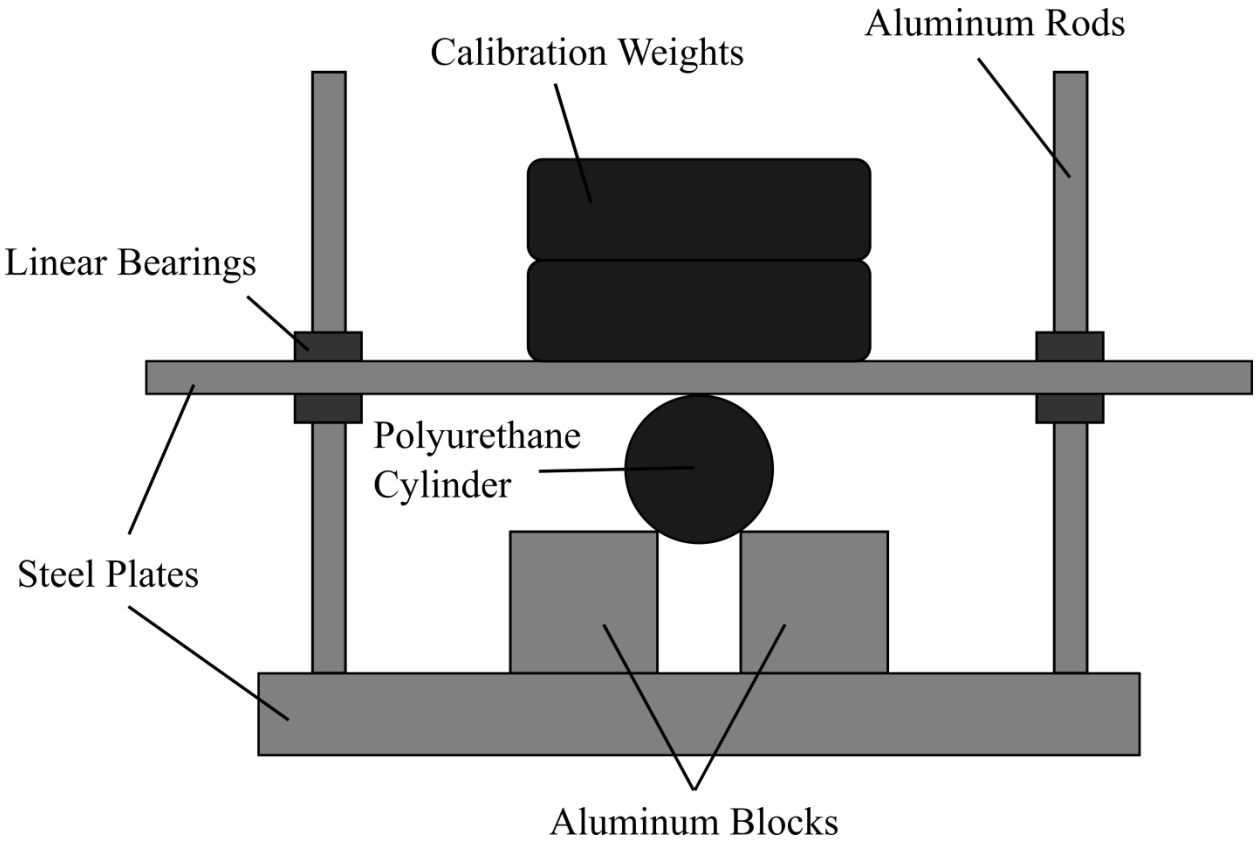

Fig. 4. The apparatus consists of a steel plate mounted on four rods and a polyurethane cylinder which rests on two aluminum bars. Load was applied by setting calibration weights on the top steel plate which moves freely in the vertical direction.

The elastic modulus was determined for each of the polyurethane cylinders using an analytical solution which describes the compression of a cylinder onto a plane [19] given by

$$\alpha = \overline{P} \cdot \left(V_1 + V_2\right) \cdot \left[1 + \ln\left\{\frac{8a^2}{\left(V_1 + V_2\right) \cdot \overline{P} \cdot D}\right\}\right] \tag{6}$$

$$V = \frac{1 - \nu^2}{\pi E} \tag{7}$$

where 2α is the total compressed distance when loaded between two planes, $\overline{P}$ is the load per unit length, 2a is the length of the cylinder, D is the diameter, and V is a material constant. Because

the steel plates have a much higher elastic modulus than the polyurethane, V_2 was assumed to have a negligible effect and is ignored. Compression tests were conducted on each of the polyurethane cylinders using the experimental apparatus without the blocks present. An image was taken of each cylinder before compression to calibrate the ImageJ software followed by an image of each cylinder compressed with a known load. The elastic moduli for the three polyurethane cylinders were calculated to be 1.1 ksi, 2.0 ksi, and 2.7 ksi, each having a Poisson ratio of 0.49. Fig. 5 shows the penetration being measured of a sample in ImageJ. The images were then calibrated using the known distance between the two aluminum blocks. Because each of the three cylinders had some warping, the penetration was measured for each trial four times at rotational angles of 0°, 90°, 180°, 270°. The order of data collection was randomized to address stochastic variation and potential anisotropy in the cylinder behavior.

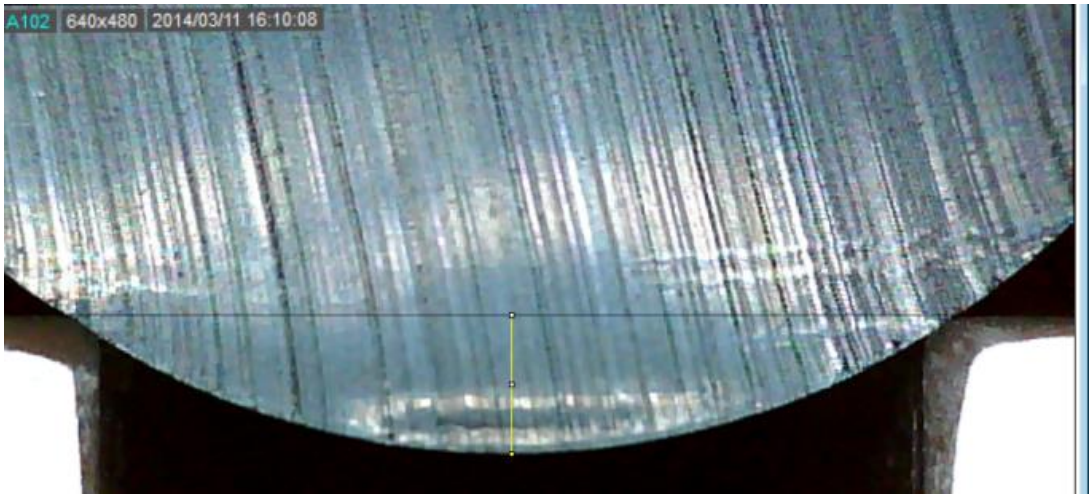

Fig. 5. Cylinder 3 loaded with 7 lb on gap size *b/R* = 1.0 as measured by ImageJ.

2.3 Results and Discussion

The computational algorithm developed for the infinitesimal spring concept was implemented with several combinations of *R* and *b*. Using a least squares regression on the results from the algorithm, the relationship between load, *P*, and penetration, δ, was determined to be

$$\delta = m \cdot P^{2/3} + n \tag{8}$$

where *m* and *n* are fit parameters which depend on cylinder radius and groove width. The penetration data for each combination of *R* and *b* resulted in a very high correlation ($R^2 > 0.99$) to (8) as seen by Fig. 6.

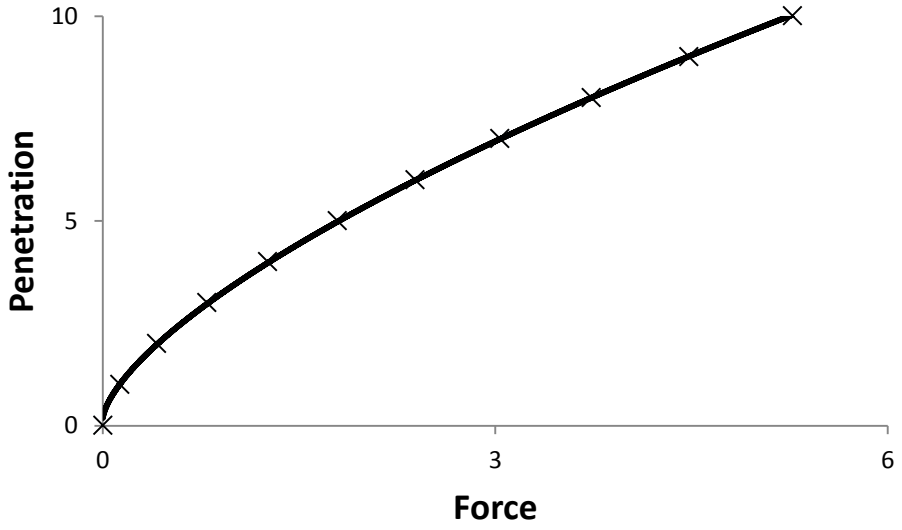

Fig. 6. The algorithm which implements (4) was tested with R=100 and b/R=0.03 and the results are denoted by 'x'. The regression shown by (8) represents this data with high accuracy ($R^2 = 1$).

When examining the penetration data from the FE simulations, the relationship between load and penetration was isolated by examining each *b/R* case individually. By conducting a

least squares regression of each *b/R* case, a power relationship was determined between loading and penetration with the best fit ($R^2 = 1$) case resulting with an exponent varying between 0.6 and 0.7. Because the parallel-infinitesimal spring concept resulted in an exponent of $2/3$, the following relationship was applied to each *b/R* case from the FE simulations.

$$\delta_f / R = K \cdot \left(p / E \right)^{2/3} \tag{9}$$

This resulted in a correlation coefficient of over 0.99 for each *b/R* case. The parameter *K* varied linearly between groove sizes. The effect of *b/R* on forced penetration was isolated by using a constant load to cause the cylinder to penetrate into grooves of varying *b/R* values. Fig. 7 shows that the forced penetration is linearly dependent on *b/R* . Incorporating this linear relationship into (9) results in

$$\delta_f / R = K \cdot b / R \cdot \left(p / E \right)^{2/3} \tag{10}$$

The value of *K* was found to be 1.282 using a least squares regression resulting in the following model for the overall cylinder penetration into the central groove:

$$\delta_{tot} / R = 1.282 \cdot b / R \cdot \left(p / E \right)^{2/3} + \delta_i / R \tag{11}$$

Fig. 8 shows the results from the model overlaid with the data collected from each FE simulation and indicates a strong correlation ($R^2 = 0.992$).

Fig. 9 shows the penetration results of the physical validation experiment using a *b/R* value of 0.5 compared with the predictions from the FE penetration model as a function of load. When loading is kept constant, the penetration can be seen as a function of *b/R* as seen by Fig. 10.

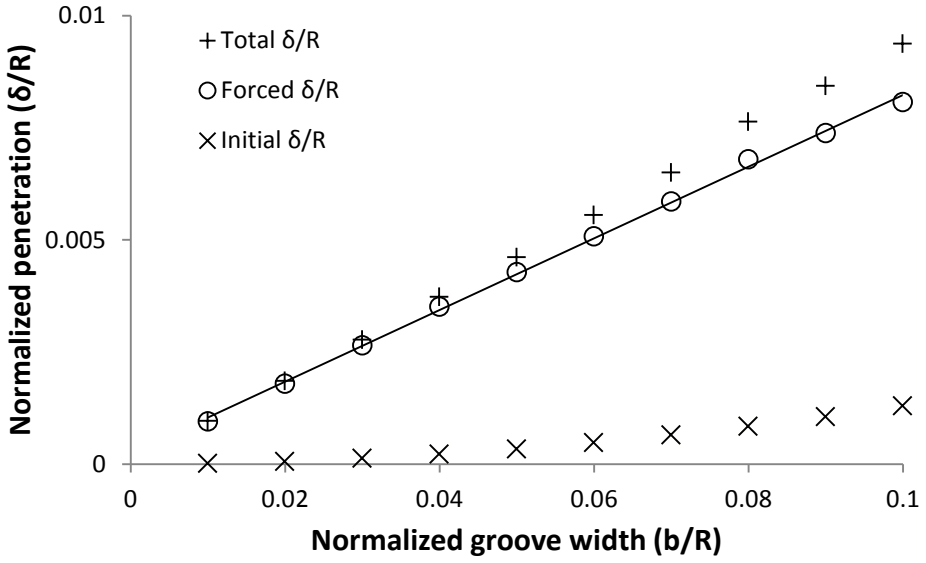

Fig. 7. The total penetration, as recorded by computational simulation, with respect to groove size when *p/E* is kept constant at 0.017. There is a highly linear relationship between groove size and penetration due to load.

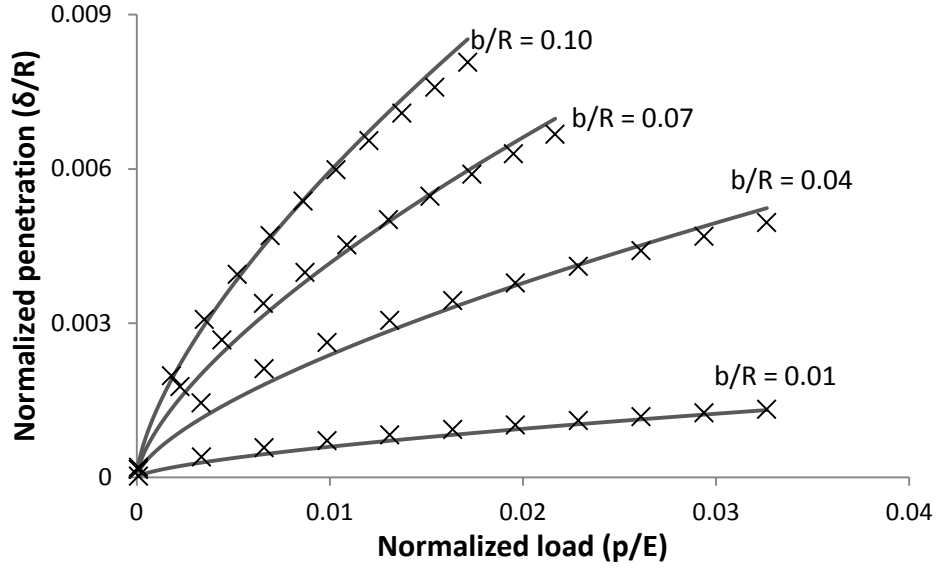

Fig. 8. Penetration as a function of *p/E* and *b/R*. Data from individual simulations are represented by data points and overlaid with results from the model.

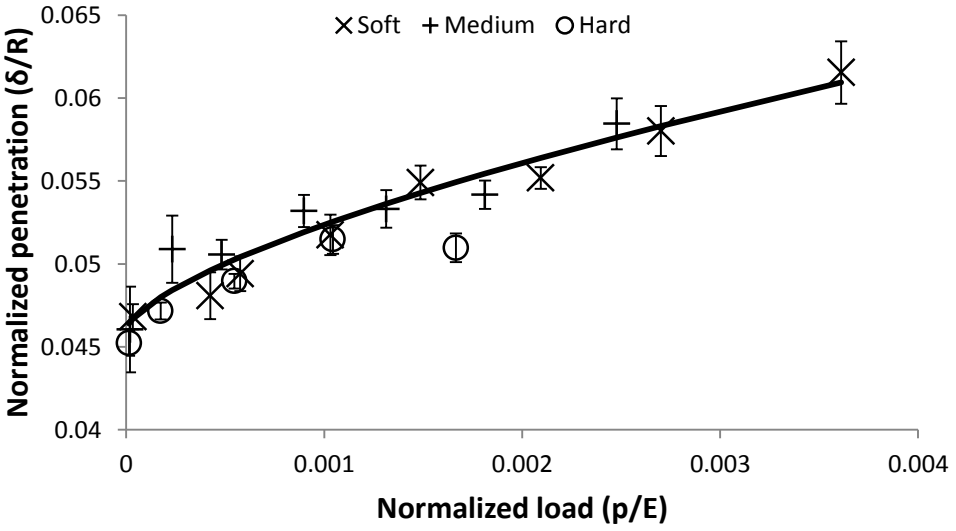

Fig. 9. Model prediction for normalized penetration compared with experimental penetration results of three polyurethane samples of varying elastic modulus into a gap of *b/R* = 0.5.

The correlation factor calculated between the model and the experimental data for *b/R* values of 0.12, 0.5, and 1.0 are 0.83, 0.91, and 0.91, respectively, showing that the model predicted penetration with high accuracy. The simulations with the smallest groove-to-radius ratio (*b/R* = 0.12) was likely the least accurate because of a higher sensitively to both the tolerance of parallelism between the two blocks and the slight warping of the polyurethane cylinders. Another important point to consider is the relatively high elastic modulus of the polyurethanes. This caused the forced penetration to be relatively small compared to the extent of penetration seen in the FE simulations. Fig. 10 clearly shows that the total penetration of the experiment is dominated by the initial penetration. Future experiments with increased *p/E* values would be useful in validating the model further so that there would be a greater amount of forced penetration.

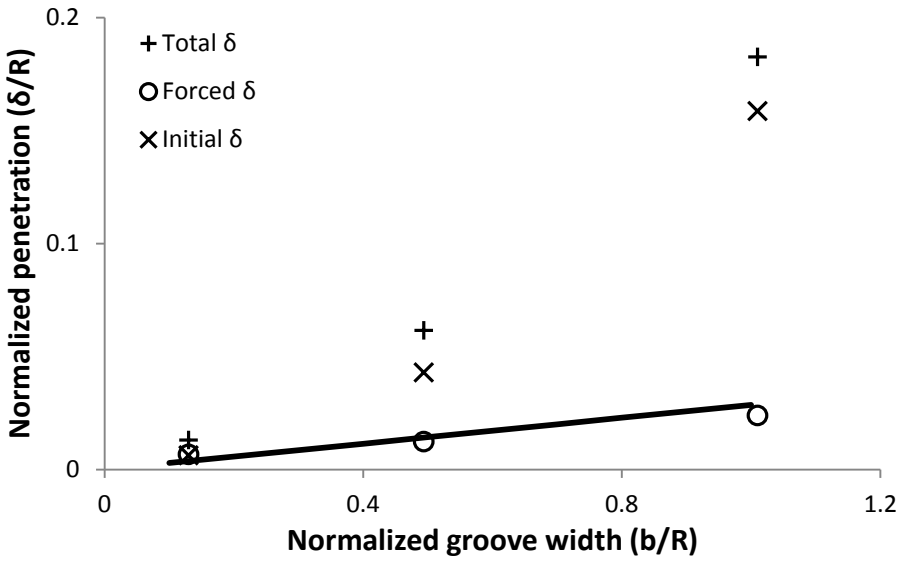

Fig. 10. The experimental penetration as a function of *b/R* with a constant *p/E*. The total penetration of the experiment is dependent mostly the initial penetration due to the relatively high values elastic modulus.

Geometrically, the initial penetration is dependent on the groove width to the power of 2 which led to the hypothesis that forced penetration would follow a similar trend. However, the forced penetration increased linearly with respect to groove width when load was kept constant. This finding led to the model developed in (11). In order to address the difficulties in modeling sharp corners with finite element methods, the model incorporated a small radius of curvature of the ridge edges (a ratio of ridge-edge radius of curvature to the radius of the deformable body of 0.001). It was assumed that the corners' contribution to forced penetration was negligible. The change in initial penetration from varying radii of curvature of the groove edges was accounted for by (1).

Additional simulations were conducted to determine the effect of additional grooves on the penetration into the center groove. Thus, a new parameter representing the width of a ridge was introduced into the model (denoted by *a*) and normalized to the cylinder radius by *a/R*. In

these simulations, *b/R* ratios of 0.01, 0.02, and 0.03 were chosen as well as *a/R* ratios of 0.012, 0.022, and 0.032. These parameters were used with simulations of 3, 5, and 7 grooves. The presence of additional grooves resulted in an increase in penetration into the center groove. The increase in grooves had a greater impact on penetration with larger *b/R* values and lower *a/R* values as seen by Fig. 11. While the shift from 1 groove to 3 grooves showed a significant impact on penetration, the increase to 5 and 7 grooves resulted in a negligible increase in penetration for the given loading range. Thus, the amount of penetration into a surface with a large number of grooves can be accurately predicted by only modeling the grooved surface as having 3 grooves. It is hypothesized that increasing the groove count above 3 may have an impact on penetration into the center groove for higher loads or a higher ratio of *b/R* to *a/R*.

As previously mentioned, Darden et al. [10] investigated the sliding of a neoprene sphere across parallel ridged surfaces of varying groove width, ridge width, and ridge height. Although the model presented in this paper assumed a cylindrical shape for the deformable body, it provides insight to their results by predicting whether the neoprene sphere is in contact with the bottom of the grooves. When the groove and edge widths were normalized with the radius of the neoprene ball, the *b/R* values varied between 0.007 and 0.05 while the *a/R* values varied between 0.012 and 0.04. In their experiment, a force of 7N was applied to the neoprene ball. The *p/E* value used in their experiment was found by doing a similar compression tests on the neoprene ball and utilizing ImageJ to find the compression and therefore an elastic modulus. The compressive stiffness of the neoprene ball was found to be 1.4 ksi which results in a *p/E* value of 0.003. Applying the model derived in this paper, which only takes into consideration one groove, it was found that penetration would be between 30%-45% of the ridge heights. However, the effect of additional grooves in this paper for a *b/R* value of 0.03 led to a fourfold

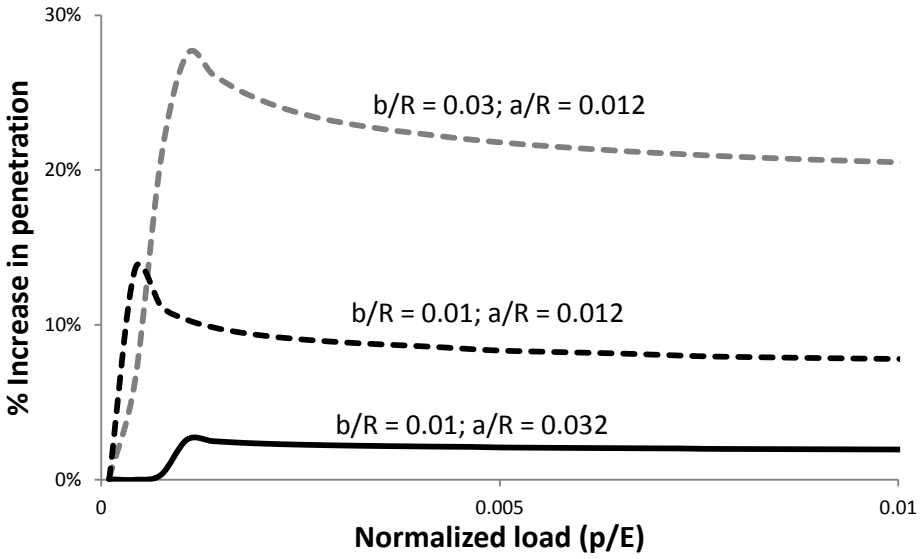

Fig. 11. When the number of grooves is increased from 1 to 3, the increase in penetration is more significant for larger *b/R* ratios and smaller *a/R* ratios. The increase in penetration grows significantly as the cylinder penetrates into the adjacent grooves but levels off after contacting the outer edge of the adjacent grooves.

increase in penetration at *p/E* value of 0.003. This suggests that with shorter ridge heights, the directionality of sliding friction is reduced because the penetration is sufficient to contact the bottom surface of the groove, providing additional contact area for adhesive friction.

This model is also insightful when compared to the findings of Tomlinson et al., whose work showed that at shallow groove depths adhesion was still the dominant mechanism, but at deep depths, the interlocking term was much more pronounced. The model can be used to bridge the gap of determining at what depth the friction mechanisms would change so as to more accurately model tactile friction. In addition, Taylor and Lederman [11] showed that penetration was of importance to tactile perception. Having an accurate prediction of penetration may be an indicator of the perception of roughness.

Future work with computational models similar to that used in this study may involve sliding the deformable cylinder over the parallel grooves with a compressive load as opposed to

the current static compression. Utilizing a sliding step with frictionless surfaces, the frictional force due to deformation and penetration could be investigated computationally and correlated with groove size and compressive load. The physical experiment could also be improved in the future by using deformable cylinders of a very fine degree of warping and also ensuring a very small tolerance of parallelism of the groove edges in addition to incorporating sliding motion.

2.4 Conclusion

- The finite element computational model results suggest that groove penetration can be very well modeled by a simple non-dimensional relationship that incorporates the ratios of groove width to cylinder radius, applied load per unit area to elastic modulus, and initial geometry-based unloaded penetration. This empirical relationship allows for penetration to be incorporated into skin friction models based on interlocking with textural features.
- The model showed a good correlation with the experimental data obtained from polyurethane cylinders loaded onto a single groove. Error was expected due to the slight warping of the cylinders, parallelism of the aluminum blocks, precision of ImageJ, and the relatively low amount of total penetration due to forced penetration.
- Elastomer penetration into a center groove is increased by the presence of additional parallel groves, as would be encountered in a uniform parallel-ridged texture. An increase in number of grooves beyond three had a minimal effect for the elastic modulus, load range, groove and ridge widths investigated here.

CHAPTER III

PARAMETRIC INVESTIGATION OF SOFT-BODY CONTACT WITH PARALLEL-RIDGE TEXTURED SURFACES TO UNDERSTAND INFLUENCE ON CONTACT AREA

A paper to be submitted to *Tribology International*

T.J. Wilde, C.J. Schwartz

3.1 Introduction

Tactile interaction with the surface of engineered products is a nearly continuous occurrence and there is a need to better understand the tactile phenomenon to improve both functional and aesthetic qualities of surface textures. Tactile interaction helps us make judgements about materials [1-3], allows us to distinguish between materials [4], and serves functional purposes such as the control of friction for product grip. Many surfaces are textured with grooves to influence the frictional characteristics of the surface. Grooved textures can be seen in products requiring grip for functionality such as power tools, razors, and bottle tops. In addition, grooves may be present on products to reduce the coefficient of friction such as some laptop mousepads, or to enable a user to tactually distinguish between surfaces such as with smartphone devices which have different surface textures for distinguishing between buttons.

The friction between a deformable body such as skin and a counter surface has been shown to be dependent on adhesion, deformation, and interlocking. In tactile friction, the adhesion component has been shown to contribute most of the frictional force [5, 6]. However, as surface roughness increases beyond a certain point, the deformation and interlocking components drive friction [9]. The contact between cylindrical bodies and rigid planes has been extensively studied to serve as a model for many applications on the micro and macro scale of

tribo-surfaces. Analytical solutions for contact area between two elastic bodies go back to Hertz and are used frequently for estimating real contact area and friction. Two and three dimensional finite element analysis (FEA) simulations have been employed for more complex surface interaction and material properties to address the complexity of modeling human skin-to-surface interactions. Jackson et al. [20] simulated the contact area of elasto-plastic hemispherical contact against a rigid flat surface. Xydas et al. [15] simulated the contact of a non-linear elastic hemispherical body against a rigid flat surface with friction. Locations of stress concentrations with respect to tactile sensors were simulated by Maeno et al. [16] for flat surfaces and by Shao et al. [17] for grooved surfaces. Each of these uses of FEA provided much insight into tactile interaction that would have otherwise been very difficult to study analytically.

Both Lederman et al. [13] and Smith et al. [12] investigated parallel-rectangular ridged textures and reported a correlation between the perception of roughness and the groove width and pressing force. Grooves were also shown to be important for grip by Tomlinson et al., whose study showed that when the surfaces roughness of triangular-ridged textures increased beyond a certain threshold, friction increased significantly as a result of interlocking [9]. In a study by Taylor et al. [11] involving a parallel rectangular ridged texture, they hypothesized that the amount of penetration of the human finger into the groove impacted the perception of surface roughness. It was hypothesized in this investigation that the number of ridges in contact plays an important role in friction and tactile perception, as it affects the real contact area and the number of instances of penetration into the grooved texture which are essential to adhesive and interlocking friction respectively. However, there lacks an analytical solution to accurately predict the number of ridges that would be in contact with an elastomeric cylinder loaded against a textured surface. Hertzian contact accurately predicts the contact distance between a soft

cylinder and rigid plane. This contact distance can be used to predict the number of theoretical ridges in contact (based on groove and ridge width), but it is analytically difficult to determine how the presence of grooves affects the contact distance with the cylinder.

The objective of this study was to determine if the presence of surface texture and its governing parameters influences contact distance to an extent that Hertzian contact can no longer be assumed. Furthermore, it is important to estimate the number of grooves in which an elastomeric body penetrates for the development of an interlocking friction model. In this investigation, numerous two dimensional FEA simulations were conducted to examine the compression of an elastic cylinder against a rigid, parallel rectangular ridged texture in order to obtain a regression model which predicts the number of ridges which are in contact for a given set of texture and loading parameters. The texture is defined by the widths of both its ridges and grooves while the cylinder is defined by its radius and elastic modulus, and is taken to be incompressible. The input parameters of similitude for the model were non-dimensionalized so that the model could be applied to both the micro and macro scale.

3.2 Method

3.2.1 Texture parameters and application to Hertzian contact

The textures used in this analysis were two dimensional and having the cross section of parallel rectangular ridges, as indicated in Fig. 12. The texture's ridge width is referred to as *a,* while the distance between the ridges, or the texture's groove width, is referred to as *b*. A cylinder was used to represent the elastomeric body because its geometry is seen in many applications and its simple nature confines its defining parameters to its radius, *R*, elastic

modulus, E, and Poisson ratio, ν. The applied load per unit area of the cylinder is referred to as *p*. The number of the central ridge edges which come into contact with the cylinder when loaded is referred to as *Q*. The parameters of similitude were non-dimensionalized using Buckingham Pi theorem to be *a*/*R*, *b*/*R*, and *p*/*E*, respectively.

In order to examine if the Hertzian model was an adequate prediction for determining the number of ridges of a textured surface in contact with the elastomeric cylinder, a relationship was needed to define Hertzian contact distance in terms of the texture parameters. Generally, a formulation of the Hertzian contact distance between a cylinder and two rigid plates includes a loading term per unit depth. Adjusting this formulation to include *p*, and in terms of the radius yields the following

$$d = 4R\left(p\frac{2}{\pi}\frac{1-\nu^2}{E} \right)^{1/2} \tag{12}$$

In order to use the Hertzian model to predict the number of ridge edges in contact, (12) needed to be expressed in terms of number of ridges, *Q*, and texture parameters *a* and *b*. In order to accomplish this, the Hertzian contact distance needed to be defined in terms of a virtual ridge-count distance, denoted as *Q'*. This virtual ridge-count distance describes contact distance solely on the number of inner ridge edges in contact and is equal to *Q* at the instant the cylinder initiates contact with a new pair of central ridge edges. Because the center of the cylinder was constrained to align with the centerline of the central groove, it was initially in contact with two ridge edges when unloaded, or had an initial contact distance of *b*. The difference of the initial contact distance from the total contact distance is of interest because it determines the number of additional ridge edges in contact when divided through by the pitch of the ridges, or *a*+*b*. This relationship is described by

$$Q' = 2 + \frac{d - b}{a + b} \tag{13}$$

Fig. 12 depicts each of these governing parameters and shows how the number of central ridge edges in contact can be determined to be 4, based on the additional contact outside of the center groove summing to slightly higher than two times the pitch.

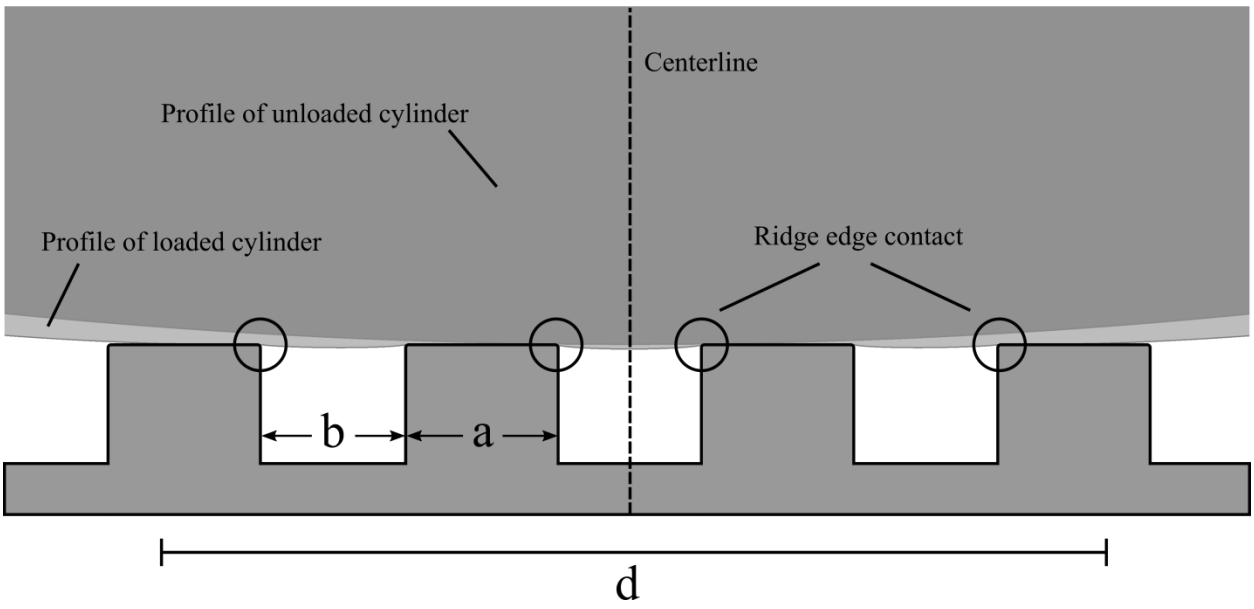

Fig. 12. Geometry of a grooved texture where 'd' is the contact distance, 'a' is the ridge width, and 'b' is the groove width. The unloaded cylinder is in initial contact with 2 ridges, or *Q* = 2. After loading, *Q* increases to 4 and can be predicted by the Hertzian contact distance.

Substituting (12) into (13) and putting into dimensionless parameters, yields

$$Q' = 2 + \frac{-b/R + 4\sqrt{\frac{2}{\pi}}\left(1 - v^2\right)^{1/2}\left(p/E\right)^{1/2}}{a/R + b/R} \tag{14}$$

The virtual ridge-count contact distance is more practical when it is expressed as a concrete number of ridge edges in contact, or *Q*. This was accomplished using a floor function. Because *Q* represents the number of ridge edges in contact, it must be an integer, and because the model

is symmetric in the lateral direction, the number must be even. Thus, the floor function must round down to the nearest even integer. The mathematical representation for a floor function to the nearest integer is expressed by the brackets "⌊ ⌋". Assuming an incompressible material (ν = 0.5), the Hertzian model for number of ridge edges in contact is then

$$Q = 2\left\lfloor 1 + \frac{-\frac{1}{2}b/R + 1.382\left(p/E\right)^{1/2}}{a/R + b/R} \right\rfloor \tag{15}$$

(15) is the finalized form of the Hertzian-based ridge prediction model and will hereafter be referred to as the 'Classic Hertzian Model'. This model was used as a benchmark to investigate the accuracy of the more complex regression-fitted models based on finite element analysis, described below.

3.2.2 Finite element method

A two dimensional finite element method was utilized (Abaqus/CAE v6.12) to run several experiments efficiently. Plain strain elements were used to better model a cylinder by assuming the strain in negligible outside of the plane. An 8-node biquadratic quadrilateral element was used with full integration. Quadratic elements assisted in simulating contact of curved surfaces to a higher degree and the use of full integration reduced the effect of hour-glassing. The experimental validation of this computation model was presented in a previous paper (under review).

In order to verify the simulation configurations as well as the classic Hertzian contact approximation (15), the cylinder was first loaded between two flat rigid plates. The resulting contact distance was recorded as a function of load and converted to *Q'* values using (13). These

values were then compared to the predictions from the classic Hertzian equation (15) to verify (13) and (15) as well as the simulation configurations.

The cylinder was then centered and rested on a rigid grooved surface. The mesh was highly refined in the area of contact as depicted by Fig. 13 to increase the accuracy at which the cylinder made contact with additional ridge edges. The load was large enough such that an adequate number of ridges are initiated into contact with the deformable cylinder. The exact load was noted when each ridge became in contact during the loading process. This process was repeated for all combinations of *b/R* values of 0.01, 0.02, 0.03, and *a/R* values of 0.012, 0.022,

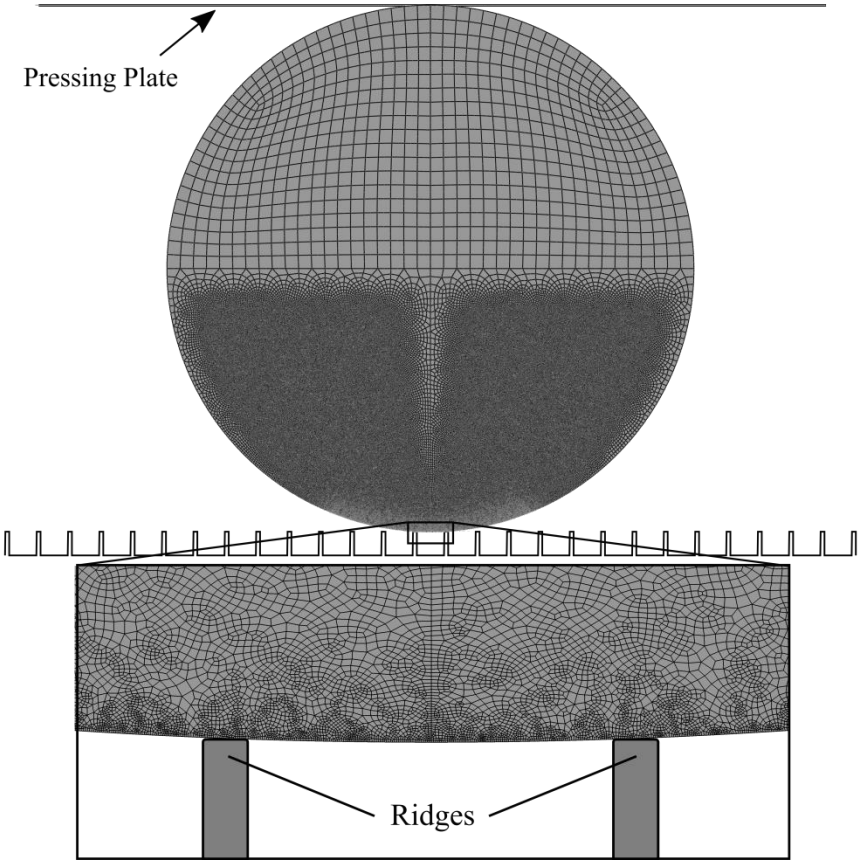

Fig. 13. FEM model with a large *b/R* of 0.09, and small *a/R* of 0.011 for display purposes. The mesh is highly refined at the area of contact.

and 0.032. These are values which are common in tactile experiments [10] when assuming a single radius of curvature to represent the finger. From the *p/E* values obtained when ridge edges became in contact, a model was developed using a least squares regression which incorporated the dimensionless geometric and loading parameters to predict *Q*.

3.3 Results and Discussion

3.3.1 Modified Hertzian Model

The finite-element (FE) based simulation model was first verified by comparing the simulated contact distance of a compressed cylinder between two rigid plates with the Hertzian contact distance approximation. Relation (2), which relates contact distance to virtual ridge-count contact distance (*Q'*), was also verified by comparing its results to the classic Hertzian contact described by (15). This comparison resulted in a high correlation ($R^2 = 1$) and maximum error of 2% which can be seen by Fig. 14.

As previously stated, the cylinder was then loaded against a rigid grooved surface for all combinations of normalized groove and ridge width, respectively (*b/R* values of 0.01, 0.02, 0.03 and *a/R* values of 0.012, 0.022, and 0.032). As normal load was increased during the FE simulations, the load at which a new pair of ridge edges came in contact with the deformed cylinder was recorded. Fig. 15 shows the number of ridge edges in contact (*Q*) as a function of non-dimensional load and ridge width, with a fixed value of normalized groove width. Ridge edge contacts can only take on even integer values, thus those are the points plotted in the figure. The number of ridge edges in contact is equal to the virtual ridge-count distance (*Q'*) when the

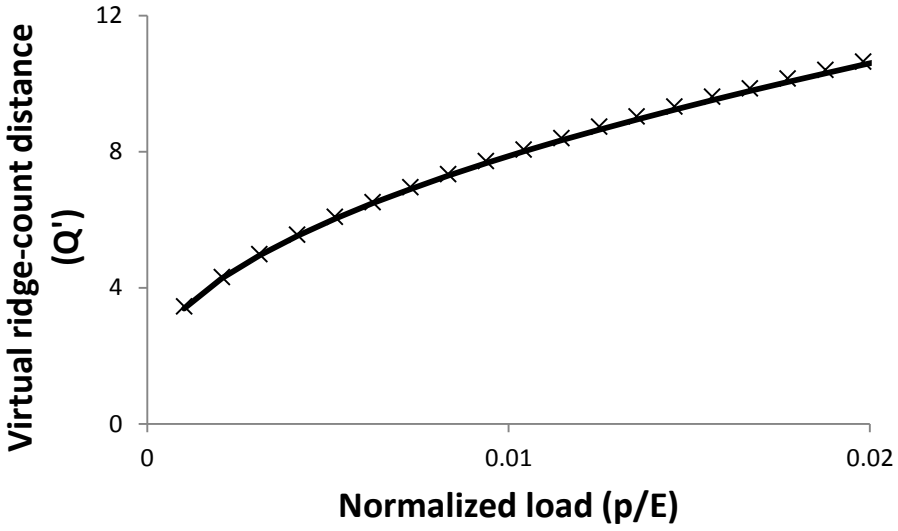

Fig. 14. Contact distance between a cylinder and two rigid planes was simulated and converted to virtual ridge-count distance (*Q'*) in contact using (13) by assigning arbitrary values of *a/R* and *b/R* to 0.022 and 0.03 respectively. The simulated results are predicted with high accuracy ($R^2 = 1$) by the classic Hertzian contact (solid line).

latter takes on even integer values (e.g., 2, 4, 6, etc.). All other parameter combinations showed similar trends. Each data series in Fig. 15 shows a relationship between loading and ridge edge contacts that can be well modeled by

$$Q = 2 + K\left(p/E\right)^{1/2} \tag{16}$$

with a high correlation for each series ($R^2 > 0.999$). Thus, K must be a function of the texture parameters, *b/R* and *a/R*. The classic Hertzian equation described by (15) takes a similar form, however, it over-predicted the amount of load necessary to obtain contact with a certain number of ridge edges. It was hypothesized that a potential contribution to this was the fact that (15) did not include an initial contact distance equal to *b*. When the Hertzian contact distance described by (12) included an initial contact distance of *b*, the first term on the numerator of (15) vanishes yielding

$$Q = 2\left\lfloor 1 + \frac{1.38}{a/R + b/R}\left(p/E\right)^{1/2} \right\rfloor \tag{17}$$

This model describes the data remarkably well ($R^2 = 0.999$) and will hereafter be referred to as the 'Modified Hertzian Model'. This relation indicates that in these particular ranges of normalized load, groove width and ridge width, respectively, the individual values of groove width and ridge width have a minimal effect because it only depends on the sum of *a/R* and *b/R*, or the pitch. Moreover, this best fit model is nearly identical to the classic Hertzian contact described by (15) when the initial contact distance is accounted for as previously described.

The Hertzian model under-predicted the necessary load to initiate contact with 4 ridge edges at relatively small groove widths (*b/R*). This was because of the inherent error in the FE simulation due to the size of the calculation increment. Because contact with four ridge edges required very little applied load, the simulation added more load than necessary to obtain the

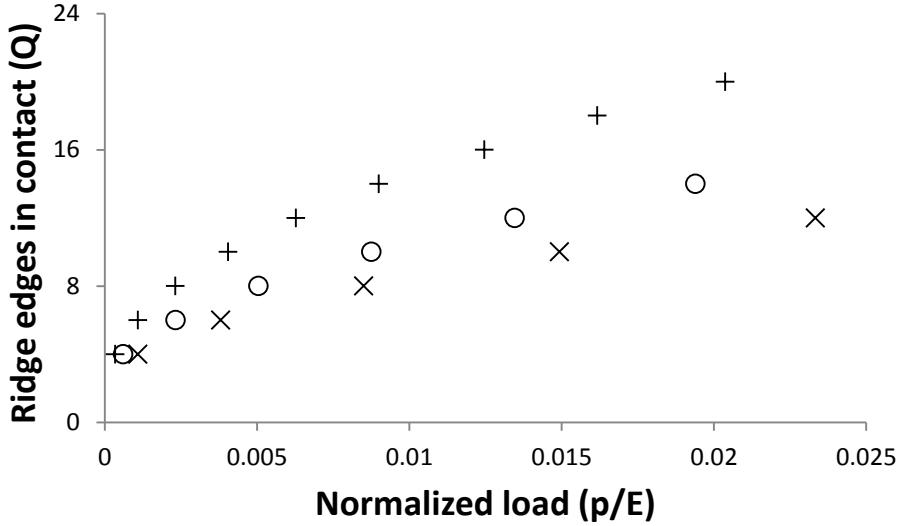

Fig. 15. Number of ridge edges in contact as a function of load. The *b/R* value is kept constant at 0.01 while *a/R* is varied from 0.032 (x), to 0.022 (o), and 0.012 (+). Decreasing *b/R* with a constant *a/R* value follows a similar trend.

contact. However, the increment is small enough to give much more accurate loads for contact with six or more ridge edges at low *b/R* ratios.

3.3.2 Hybrid Model

The error of the Modified Hertzian Model increased as groove width increased or ridge width decreased. At the lowest *b/R* to *a/R* ratio, 0.01 and 0.032 respectively, the error of the Modified Hertzian Model was between 1% and 2%, while at the highest *b/R* to *a/R* ratio, 0.03 and 0.012 respectively, the error climbed to between 3% and 5%. This can be attributed to a deviation from classic Hertzian contact as penetration into the grooves becomes more profound. With a normalized groove width (*b/R*) much larger than normalized ridge width (*a/R*), (values of 0.09 and 0.012 respectively) the error in predicted load of the Modified Hertzian Model grows to as high as 15% compared to the FE simulation. Thus, it was decided to consider an additional term in the model to address this issue. Because it was seen that larger ridge widths caused more hindrance to ridge-edge contact than did groove widths, an additional term dependent on normalized ridge width (*a/R*) was added to the existing model to account for this difference. Using a least squares best-fit regression, the empirically modified model became

$$Q = 2\left\lfloor 1+\left\{\frac{1.348}{a/R+b/R}+\frac{0.01583}{a/R}\right\}\left(p/E\right)^{1/2}\right\rfloor \tag{18}$$

hereafter referred to as the 'Hybrid Model'. There are two terms in the coefficient to the load. It is heavily influenced by the first term, which is effectively the normalized pitch of the texture. As the pitch increases, the number of ridge edges in contact decreases. The second term, which is only dependent on *a/R*, represents the resistance to deformation caused by the width of the

ridges. In contrast to *b/R*, *a/R* increases both the pitch and resistance to compression, thus having a more profound effect on limiting *Q*. The predictions from the Hybrid Model were compared to that of the Modified Hertzian Model for all FE simulations. The Hybrid Model performed even better than the Modified Hertzian Model at the lowest *b/R* to *a/R* ratio as shown by Fig. 16. As the *b/R* to *a/R* ratio increased, the Hybrid Model remained within 2% error while the Modified Hertzian Model became less accurate, as shown by Fig. 17. Furthermore, while the error of the Modified Hertzian Model grew to 15% for the highest *b/R* to *a/R* ratio tested, the Hybrid Model remained below 2% in error.

For larger *b/R* values, it became more difficult for FE simulations to converge to obtain contact with a large number of ridges. A suggestion for future simulations is to conduct controlled displacement simulations rather than controlled load to increase the likeliness of convergence.

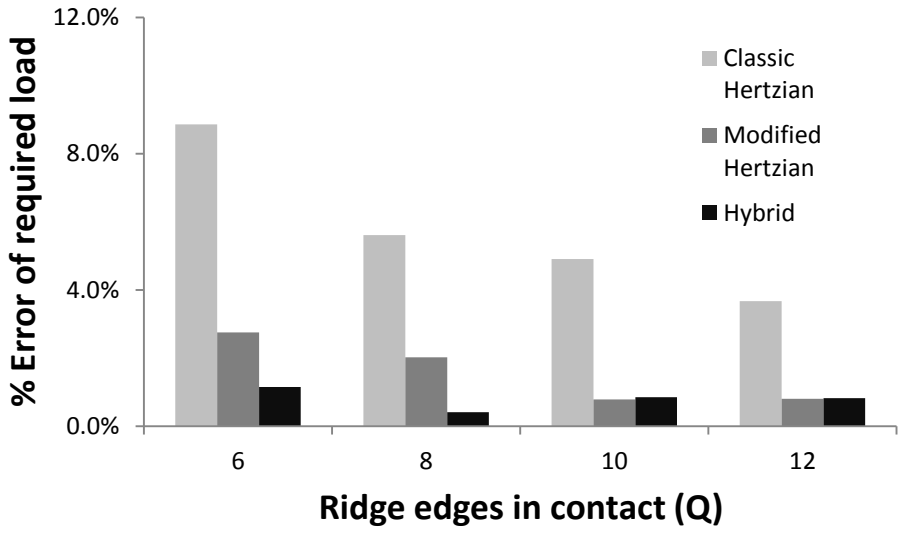

Fig. 16. Percent error of required load for number of ridge edges in contact for small groove width (*b/R*=0.01) and large ridge width (*a/R*=0.032). The classic Hertzian equation and the Modified Hertzian Model are relatively accurate but outperformed by the Hybrid Model.

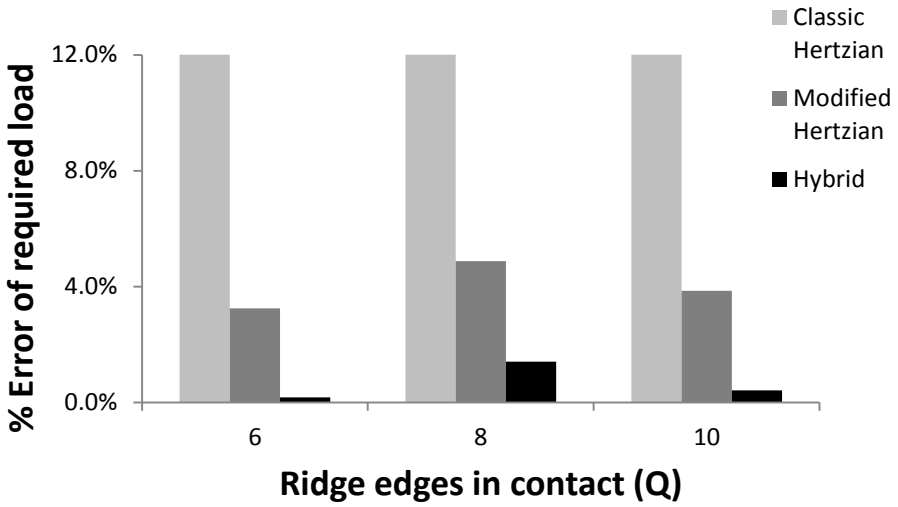

Fig. 17. Percent error of required load for number of ridge edges in contact for large groove width (*b/R*=0.03) and small edge width (*a/R* = 0.012). At these higher ratios of *b/R* to *a/R*, the Hertzian prediction and the Modified Hertzian Model becomes much less accurate while the Hybrid Model, which incorporates the individual values of *a/R* and *b/R*, remains highly accurate.

The effect of the presence of grooves on the compression of the cylinder and theoretical contact distance was contrary to the authors' original expectations. It was previously hypothesized by the authors that the presence of grooves would inhibit the horizontal growth of contact with the grooved surface and larger grooves would further this inhibition because of the area of the cylinder that would subsequently be penetrating into the grooves. However, the result was the opposite. The presence of the grooves and the allowance for penetration results in a reduction in resistance to compression. This allows the cylinder to be compressed to a greater extent for a given load than if it was loaded against a rigid plane. This effect was more prominent for *b/R* values over 0.3, above which the Hertzian contact begins to greatly over predict the amount of load necessary to obtain contact with a certain number of ridge edges.

The model displayed by (18) is useful to predict the real contact area between a cylindrically shaped elastomeric body with a parallel grooved texture. Furthermore, this model is

important to the development of an interlocking friction model as it determines the number of grooves in which the elastomeric body penetrates the texture. As previously mentioned, Taylor and Lederman found penetration into grooves to be an important contribution to the deformation component of friction and Tomlinson et al. [9] found interlocking to be the dominant component of friction with triangular-ridge textures of high surface roughness. Furthermore, the groove widths and pressing force were linked to the perception of roughness by Smith [12] and Taylor [11]. Therefore the perception of roughness may also be linked to the number of ridges in contact as this number increases with load. Additional research may be warranted to observe the stresses induced on the cylindrical body by the individual ridges such as seen in the work of Shao et al. [17]. The model developed from this investigation would provide the number of locations of these stress sites from groove ridge to finger interaction which may provide insight on tactile perception.

3.4 Conclusion

- Classic Hertzian theory does a reasonable job of predicting the number of ridge-edge contacts when an elastomeric cylinder is loaded against a parallel-rectangular-ridge texture, so long as normalized groove size is relatively small (*b/R* below 0.01) and normalized ridge width is sufficiently large (*a/R* above 0.032). Outside of these parameter ranges, the model exhibits considerable error.
- A Modified Hertzian model, which takes into account the pitch of the texture ridges, predicted the loads required to obtain a specified number of ridge-edge contacts with the specified ranges of *b/R* and *a/R* with high accuracy. This model becomes less accurate,

however, with large groove widths because penetration into the grooves becomes more substantial and has an impact on overall penetration of the cylinder into the texture grooves.

- A Hybrid model was developed which introduced empirical fit into the Modified Hertzian model, and was structured to include both pitch and ridge width. This model was highly accurate with all values tested of b/R and a/R, including extreme ratios between the two texture parameters.

CHAPTER IV

GENERAL CONCLUSIONS

Understanding tactile friction with textured surfaces is extremely important to properly design and engineer products to meet their functional purposes. While it has been shown that the presence of surface texture can increase friction due to deformation and interlocking mechanisms, the effect of surface geometry and loading is poorly understood.

Interlocking friction between an elastomeric body and a textured surface occurs from the penetration of the elastomeric body between the ridges of the texture when the surfaces become in contact. Furthermore, the extent of penetration determines the amount of micro-adhesion which occurs from contact with the bottom of groove channels. Although difficult to model this contact mechanics problem analytically, the advent of finite element analysis allowed for the collection of data from several computational simulations from which regression models could be obtained. These models proved to predict with high accuracy both the number of ridges that become in contact and the extent of penetration that occurs based on dimensionless parameters which describe the loading and geometry conditions. To more thoroughly investigate the relationship between penetration and amount of ridges in contact with interlocking friction, it would be very beneficial to conduct sliding simulations and experiments to better understand how friction can be controlled by textural properties.

REFERENCES

1. Chen, X., et al., *Materials' tactile testing and characterisation for consumer products' affective packaging design.* Materials & Design, 2009. **30**(10): p. 4299-4310.

2. Childs, T.H.C. and B. Henson, *Human tactile perception of screen-printed surfaces: Self-report and contact mechanics experiments.* Proceedings of the Institution of Mechanical Engineers, Part J: Journal of Engineering Tribology, 2007. **221**(3): p. 427-441.

3. Barnes, C.J., et al., *Surface finish and touch—a case study in a new human factors tribology.* Wear, 2004. **257**(7): p. 740-750.

4. Bergmann Tiest, W.M., *Tactual perception of material properties.* Vision research, 2010. **50**(24): p. 2775-2782.

5. Adams, M.J., B.J. Briscoe, and S.A. Johnson, *Friction and lubrication of human skin.* Tribology letters, 2007. **26**(3): p. 239-253.

6. Tomlinson, S.E., R. Lewis, and M.J. Carré, *The effect of normal force and roughness on friction in human finger contact.* Wear, 2009. **267**(5): p. 1311-1318.

7. Skedung, L., et al., *Finger friction measurements on coated and uncoated printing papers.* Tribology letters, 2010. **37**(2): p. 389-399.

8. Derler, S., et al., *Influence of surface microstructure on the sliding friction of plantar skin against hard substrates.* Wear, 2009. **267**(5): p. 1281-1288.

9. Tomlinson, S.E., et al., *Human finger contact with small, triangular ridged surfaces.* Wear, 2011. **271**(9): p. 2346-2353.

10. Darden, M.A. and C.J. Schwartz, *Investigation of friction mechanisms during the sliding of elastomers against hard parallel-ridge textures.* Tribology International, 2013. **63**: p. 2-7.

11. Taylor, M.M. and S.J. Lederman, *Tactile roughness of grooved surfaces: A model and the effect of friction.* Perception & Psychophysics, 1975. **17**(1): p. 23-36.

12. Smith, A.M., et al., *Role of friction and tangential force variation in the subjective scaling of tactile roughness.* Experimental Brain Research, 2002. **144**(2): p. 211-223.

13. Lederman, S.J., *The perception of surface roughness by active and passive touch.* Bulletin of the Psychonomic Society, 1981. **18**(5): p. 253-255.

14. Kawasoe, T., M. Kakizawa, and H. Shimizu, *Tribology in the hair surface and tactile perception.* Tribology Online, 2008. **3**(2): p. 127-130.

15. Xydas, N., M. Bhagavat, and I. Kao. *Study of soft-finger contact mechanics using finite elements analysis and experiments*. IEEE.

16. Maeno, T., K. Kobayashi, and N. Yamazaki, *Relationship between the Structure of Human Finger Tissue and the Location of Tactile Receptors.* JSME International Journal Series C, 1998. **41**(1): p. 94-100.

17. Shao, F., et al., *Finite element simulations of static and sliding contact between a human fingertip and textured surfaces.* Tribology International, 2010. **43**(12): p. 2308-2316.

18. Johnson, K.O. and J.R. Phillips, *Tactile spatial resolution. I. Two-point discrimination, gap detection, grating resolution, and letter recognition.* Journal of Neurophysiology, 1981. **46**(6): p. 1177-1192.

19. Puttock, M.J. and E.G. Thwaite, *Elastic compression of spheres and cylinders at point and line contact*. 1969: Commonwealth Scientific and Industrial Research Organization Melbourne, VIC, Australia.

20. Jackson, R.L. and I. Green, *A finite element study of elasto-plastic hemispherical contact against a rigid flat.* Journal of Tribology, 2005. **127**(2): p. 343-354.

APPENDIX

PARALLEL-INFINITESIMAL SPRING COMPRESSION PSEUDO-CODE MODELING THE PENETRATION INTO A SINGLE GROOVED TEXTURE

```
// Assign arbitrary radius value, maximum compression, number of springs, and half groove
// width
        R = 1;
        maxCompression = 1;
        numOfSprings = 1000;
        b = 0.01;
// Determine compression increments and resulting increments of contact distance
        for (i=0; i < numOfCompressionIncrements; i++){
                cIncrements[i] = i * maxCompression/( numOfCompressionIncrements-1)
                contactDistanceIncrements[i] = SquareRoot( 2 * R * cIncrements[i] -
cIncrements[i]^2)
        }
// Create a Spring class which is given an x location and can determine its force with a given
c and R
        class Spring {
                location x;

                // Constructor
                Spring( location){
                        x = location;
                }
                // Method to obtain force with given compression of cylinder
                getForce( c, R){
                        return 2*c – (2*R – 2*SquareRoot(R^2 – x^2)
                }
        }
// Assign spring locations based on the number of springs
        springList.add( new Spring(0)); // Center Spring
// Determine distance between springs based on Radius and numOfSprings
        distBetweenSprings = R/((numberOfSprings-1)/2);
// Loop through half the number of springs and assign an x position to two springs
        for (i=0; i<(numberOfSprings-1)/2; i++){
                spring = new Spring((i+1) * distBetweenSprings);
                springList.add(spring);
                springList.add(spring);
        }
```

```
// Sum up the resulting force at each c increment
        for (i=0; i < numOfCompressionIncrements; i++){
                // Loop through springs and check that location is less than half-contact
distance but greater than the half groove width
                for ( Spring currentSpring : springList ){
                        if (currentSpring.getLocation() > b && currentSpring.getLocation()
                        <= contactDistanceIncrements[i] ){
                                // add the force of the current spring to the total force
                                forceIncrement[i] += currentSpring.getForce(cIncrements[i],
                                R)/numOfSprings
                        }
                }
        }
```